references, see Thomlinson & Williams, 1984; Brown & Lindau, 1986).

A position-sensitive detector can replace the receiving slit when a reciprocal space is scanned. TV area detectors with an X-ray-to-visible light converter and two-dimensional CCD arrays have moderate resolution and efficiency, but they work in the current mode and do not provide pulse discrimination on the basis of the photon energy. One- and two-dimensional proportional chambers have a spatial resolution of the order of 0.1 mm, and the relative energy resolution, $\Delta E/E \simeq 0.2$, is sufficient for rejection of some of the parasitic scattering.

The NaI(Tl) scintillation counter is used most frequently as the X-ray detector in crystallography. It has 100% efficiency for the commonly used wavelengths, and the energy resolution is comparable to that of a proportional counter. The detector has a long life, and the level of the low-energy noise can be reduced to about 0.1 counts s^{-1}.

The Ge and Si(Li) solid-state detectors (SSD) have an energy resolution $\Delta E/E = 0.01$ to 0.03 for the wavelengths used in crystallography. The relative Compton shift, $\Delta\lambda/\lambda$, is $(0.024\ \text{Å}/\lambda) \times (1 - \cos 2\theta)$, where 2θ is the scattering angle, so that even this component can be eliminated to some extent by a SSD. These detectors have been bulky and expensive, but new constructions that are suitable for X-ray diffraction have become available recently. The effects of the detector resolution are shown schematically in Fig. 7.4.4.5 for a scintillation counter and a SSD.

Crystal monochromators placed in front of the detector eliminate all inelastic scattering but the TDS. The monochromator must be matched with the preceding X-ray optical system, the sample included, and therefore diffracted-beam monochromators are used in powder diffraction only (see Subsection 7.4.4.4).

7.4.4.4. *Powder diffraction*

The signal-to-background ratio is much worse in powder diffraction than in single-crystal diffraction, because the background is proportional to the irradiated volume in both cases, but the powder reflection is distributed over a ring of which only the order of 1% is recorded. The phase-space diagrams of a typical measurement are shown in Fig. 7.4.4.6. The Johansson monochromator is matched to the incident beam to provide

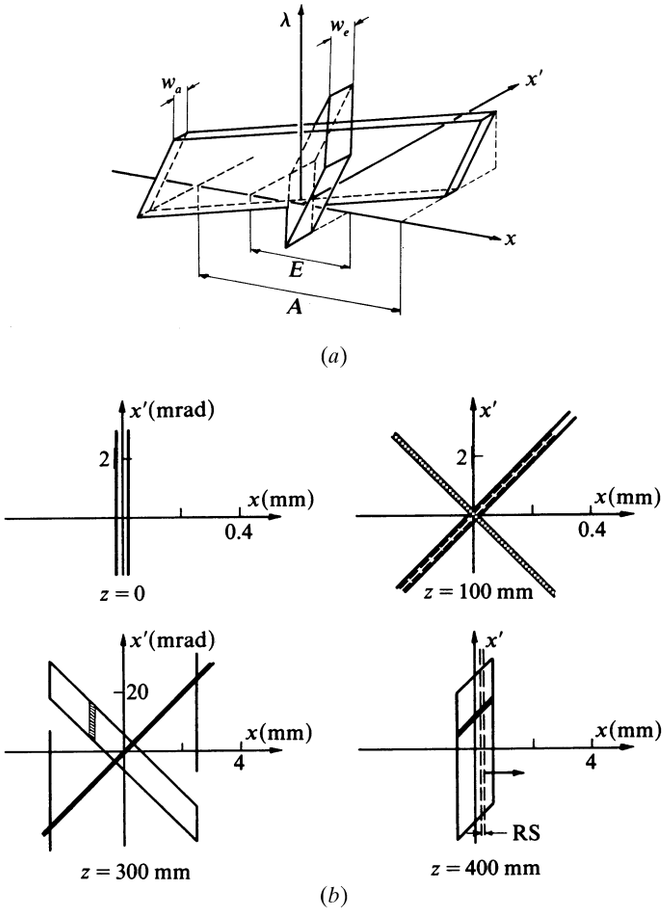

Fig. 7.4.4.6. Equatorial phase-space diagrams for powder diffraction in the Bragg–Brentano geometry. (*a*) The acceptance and emittance windows of a Johannson monochromator; (*b*) the beam in the $\lambda = \lambda_1$ plane: the exit beam from the Johansson monochromator is shown by the hatched area ($z = 100$ mm), the beam on the sample by two closely spaced lines, the reflectivity range of powder particles in a small area of the sample by the hatched area ($z = 300$ mm, note the change of scales), and the scan of the reflected beam by a slit RS by broken lines ($z = 400$ mm, at the parafocus).

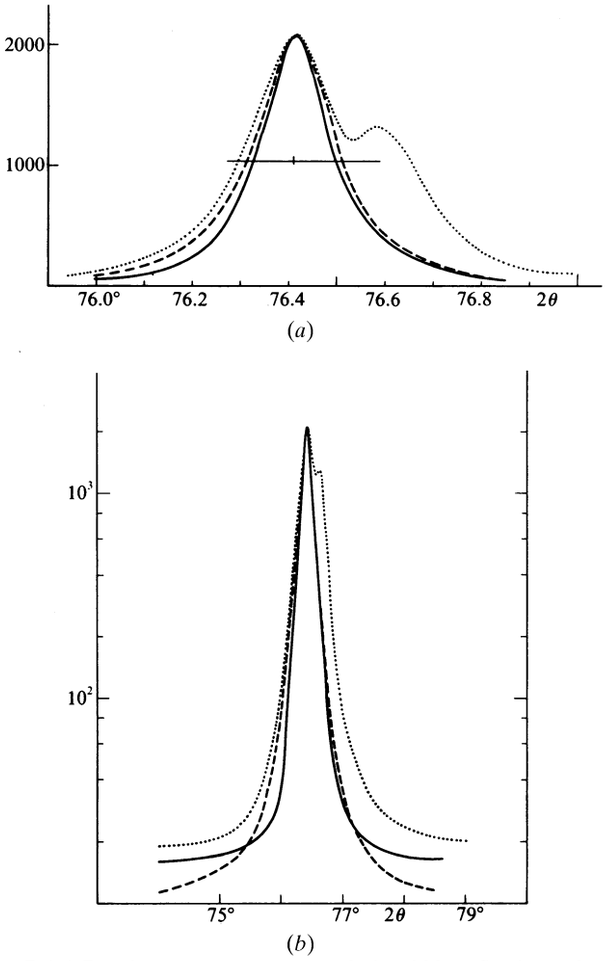

Fig. 7.4.4.7. Three measurements of the 220 reflection of Ni at $\lambda = 1.541$ Å scaled to the same peak value; (*a*) in linear scale, (*b*) in logarithmic scale. Dotted curve: graphite (00.2) Johann monochromator, conventional 0.1 mm wide X-ray source (Suortti & Jennings, 1977); solid curve: quartz (10.1) Johansson monochromator, conventional 0.05 mm wide X-ray source; broken curve: synchrotron radiation monochromatized by a (+, −) pair of Si (111) crystals, where the second crystal is sagittally bent for horizontal focusing (Suortti, Hastings & Cox, 1985). The horizontal line indicates the half-maximum value. In all cases, the effective slit width is much less than the FWHM of the reflection.

references